

SPid 10746

[Home](#) | [Dates](#) | [Call for Papers](#) | [Call for Tutorials](#) | [Video Festival](#) | [Conference Organization](#) | [Conference Program](#) | [Conference Registration](#) | [Final Submission](#) |

Accepted Papers

Conference Papers

#	Title	Authors
25748	XMegaWall: A Scalable, Super High-Resolution Tiled Display using a PC Cluster	YongBin Kang (Institute for C Interfaces)
25963	A sketch-based interactive framework for real-time mesh segmentation	Huai-Yu Wu (Institute of Automation, Chinese Academy of Science), Chunhong Pan (Institute of Automation, Chinese Academy of Science), Jia Pan (institute of automation academy of sciences), Qing Yang (Institute of Automation, Chinese Academy of Sciences), Songde Ma (Institute of Automation, Chinese Academy of Science)
25988	A Novel Scheme for Efficient Cross-Parameterization	Jia Pan (institute of automation academy of sciences), Huai-Yu Wu (Institute of Automation, Chinese Academy of Science), Chunhong Pan (Institute of Automation, Chinese Academy of Science), Qing Yang (Institute of Automation, Chinese Academy of Sciences)
26017	Attributes Processing for High Dynamic Range Images	Ming-Long Huang (National Central University), Chung-Ming Wang (National Central University)
26034	A New Interest Point Detection and Description Algorithm based on Bidimensional Empirical Mode Decomposition	Dongfeng Han (Jilin University), Wenhui Li (Jilin University)
26037	Mass-based Comparison Metrics for Motion Graphs	Mikiko Matsunaga (UC Riverside), Victor Zordan (UC Riverside)
26038	Improved error estimate for extraordinary Catmull-Clark subdivision surface patches	Zhangjin Huang (Peking University), Guoping Wang (Peking University)

SE
W

26050	3D Reconstruction, Visualization and Volume Calculation of Fruits	Lucio Jorge (Embrapa)
26096	Shadow Generation for Scenes Represented by Catmull-Clark Subdivision Surfaces	Shuhua Lai (Virginia State University), Fuhua (Frank) Cheng (University of Kentucky)
26219	Smoothed Particle Hydrodynamics on GPUs	Takahiro Harada (The University of Tokyo)
26244	Visualization of Chaotic Dynamical Systems Based on Mandelbrot Set Methodology	Jin Cheng (Zhejiang University)
26259	Geometry Image-based Shadow Volume Algorithm for Subdivision Surfaces	Min Tang (Zhejiang University)
26293	Automatically Construct Skeletons and Parametric Structures for Polygonal Human Bodies	Jituo Li (Academy of Chinese Sciences)
26342	A unidimensional track motion method for acoustic elastography images under dynamic compression	Lucio Pereira Neves (Universidade Federal do Rio de Janeiro), Ana Perini (University of São Paulo), Antonio A. O. Carneiro (Universidade Federal do Rio de Janeiro)
26364	Accurate Constraint-Based Modeling From A Single Perspective View	Manolis Lourakis (Foundation for Research and Technology - Hellas)
26385	3D As-Rigid-As-Possible Deformations Using MLS	Alvaro Cuno (Universidade Federal do Rio de Janeiro), Claudio Esperança (UFRJ), Antonio Alberto Fernandes de Almeida (Universidade Federal do Rio de Janeiro), Paulo Cavalcanti (Universidade Federal do Rio de Janeiro)
26403	Statistical Spherical Wavelet Moments for Content-based 3D Model Retrieval	Hamid Laga (Tokyo Institute of Technology)
26416	Dynamic Visualization of Geographic Networks Using Deformations	Basak Alper (University of California Santa Barbara), Selcuk Sumengen (Sabanci University), Selim Balcisoy (Sabanci University)
26524	Gps, Gis and Video fusion for urban modeling	Gaël Sourimant (Irisa / Inria), Luce Morin (Irisa / Université de Rennes), Kadi Bouatouch (Irisa / Université de Rennes)
26948	A Framework for Real-Time Animation of Liquid-Rigid Body Interaction	Melih Kandemir (Bilkent University), Tolga Capin (Bilkent University), Bulent Ozguc (Bilkent University)
26966	A tool for teaching musical metrics based on computer vision	Rodrigo Schramm (UNISINOS), Claudio Jung (Universidade dos Sinos (UNISINOS))
26974	Stratified helix information of Medial-axis-points Matching for 3D Model Retrieval	Ji Jia (Xi'an Jiaotong University), Zheng Qin (Tsinghua University), Jiang Lu (Xi'an Jiaotong University)
27003	Generating Steering Behaviors for Virtual Humanoids using BVP Control	Fábio Dapper (UFRGS), Edson Prestes e Silva Jr (UFRGS), Luciana Nedel (UFRGS)
		Carlos Cony (Universidade dos Sinos),

L.A.C. Jorge, R. Minghim, L.G. Nonato, C.I. Biscegli, E.C. Pedrino, V. O. Roda, M.S.V. Paiva

3D RECONSTRUCTION, VISUALIZATION AND VOLUME CALCULATION OF FRUITS

Abstract This work presents a methodology for the three dimensional (3D) models from 2D magnetic resonance image frames, aimed for some studies on fruits. The 3D models can be employed for precise volumetric description of objects of interest. Because the volumetric model is precise, the methodology lends itself to reliable volume calculation. As an illustration of its use in agriculture, a test case of a mango tissue collapse is used. The various parts of interest in the mango are reconstructed and their volume determined. Validation of the developed methodology was performed applying it for the reconstruction of two objects with known geometry and volumetric properties (phantoms). This gives an estimate of the error imposed by the procedure (0.15% to 2.3%), thus legitimating the methodology for 3D model reconstruction. The contributions of this work include the full description of the reconstruction process, from acquisition to visualization and manipulation, and the validation of the model formed. Additionally, its novelty in the field of agriculture opens new possibilities for researchers in that field of activity.

Keywords 3D Reconstruction, Segmentation, Visualization, Fruit Analysis, MRI, VTK

1 Introduction

In scientific visualization, many three-dimensional (3D) techniques for 2D image data analysis have been put forward and applied to various fields, opening enormous possibilities in many research areas, as well as many questions. New applications appear often, and in some of them invasive procedures may destroy parts of the very phenomenon one wishes to observe and also may disturb the measurements accuracy, such as volume. In agriculture, great effort has been put into quantifying fruit quality, including non-invasive techniques based on data collection from MRI and CT scans, those are, however, mainly 2D strategies. The potential benefit from 3D techniques in this context highlights some questions, for instance: how reliable are the models? What are the techniques suitable to evaluate fruit quality in visualization? What types of properties can be analyzed? This has been the motivation

for the union of efforts between researchers in visualization and in agriculture to develop the methodology for analysis of volumetric fruit properties. Because those properties can help interpret physical and physiological structures, we carried out an effort to define what precision could be obtained from the data collection available. The fundamental problem solved by the developed methodology can be stated as: given images collected by a MRI equipment with 0.2 cm spacing intra-slice with no spacing between slices and resolution of 256x256 pixels, what kind of error could be expected in the volume calculation if a whole process of reconstruction were to be applied without any particular processing to control approximation errors?

As a consequence of the effort, we managed to put together a methodology, uncommon to find in the literature, which comprises the whole process of creation of volumetric models, from acquisition to visualization and property calculation, going through each step. Works published in related subjects present techniques for each individual step, or a combination of two of the steps (such as segmentation and reconstruction, or reconstruction and visualization), but do not give a whole sequence of procedures, from the collection of data on the phenomenon under observation (in this case fruits) to a computational object that represents their structure. Even in those cases (as in medical images) where these techniques have been widely employed, there is little effort applied to the validation of the final model. To complete the methodology, we also provide its validation by calculating the approximation error of volume measurements.

The main contributions of this work are: the development of an effective methodology for 3D model reconstruction from MRI images devised to produce a robust and precise volumetric mesh of the reconstructed objects; the validation of such model for reliability of volume calculation; and the use of these results in the analysis of fruit problems, taking as test case the disease that motivated the effort in the first place: mango tissue collapse. An additional real life application of the developed methodology is presented, the volumetric reconstruction of a cashew nut.

In the next section we give an overview of the methodology and related work and justify for the particular choices of techniques. These techniques are described in the subsequent sections and a description of the results follows.

2 Related Work

There have been a number of methods developed to generate 3D models from 2D data. Research on these methods can be found in the field of the scientific visualization, which has been widely applied in medicine. We refer to the books edited by Fitzpatrick and Sonka [10], Kim and Horii [19] and Van Metter et al. [22] as sources of methods and references on the subject. There are examples of visualization in combination with other techniques in artificial neuron visualization and fluid dynamics, as well as dentistry [31]. Nowadays, the particular sequence of methods and parameters employed must be individually

adapted to each problem, in the case of this application on agriculture.

Three steps are required to generate 3D models, namely: data acquisition [1], image segmentation [29], [16], and 3D reconstruction [26].

The first step, data acquisition, obtains two-dimensional images from three-dimensional objects. It can be performed by a number of devices, such as CT, MRI, and microscopic photography. MRI has been used in a number of fruit studies with good results [7]. This fact and the quality and resolution of the images produced motivated its use in the present work. Several non-destructive methods to analyze and measure internal fruit defects have been presented in the literature [38]; [7]; [6]; [14]. In general, these techniques apply image processing methods that extract important features to estimate area, shape, and evolution of fruit degradation. These approaches are limited almost exclusively to two-dimensional (2D) images, impairing the analysis of three-dimensional (3D) structures, which might prove useful in certain applications. Making use of computer tomography (CT) [36] or magnetic resonance imaging (MRI) [7] devices to obtain 3D models from 2D data has been a common practice mainly in medical applications. By extending their use to the fruits analysis and other agricultural products, it may be possible to advance our understanding about some diseases and thereby aid the control of their manifestations. This is especially true where invasive procedures, such as actually slicing or dicing, are not desirable [37].

The second step of the methodology, segmentation, processes the images to identify and select elements of interest. There are many techniques in the literature devoted to image segmentation and they can be grouped into several categories: edge-based [5], [24], region-based [2], Markov random field-based [18], [4], deformable models [39], and hybrid techniques [16]. Some of these methods search for regions of interest, while some degree of similarity inside a region is used to detect its area. Other methods separate objects of interest by detecting edges that separate them. Many of them use hybrid approaches. The goal in the class of problems addressed here is to find boundaries between regions of interest as well as to describe the interior of these areas. The segmentation technique proposed in [27] and used here was a type region-based technique. One of its advantages lies in the fact that contour description is intrinsic of the process, while other region-based methods need a second pass at the detected regions to define them. Segmentation step requires the most processing time of the whole procedure, including various levels of interaction with the user to achieve good results.

The last step of the process, three-dimensional reconstruction, builds geometric models from the segmented images so that they can be used in simulation, visualization, interaction, and data analysis. In the type of 3D reconstruction known as mesh generation (MG), a model is defined by a number of cells, which could be planar cells (such as triangles) or volumetric cells (such as tetrahedrons). Classes of techniques to obtain such models include optimal [32], [23], deformable [34], and heuristic models [9], [3], the latter being the most popular. These

techniques make use of graph theory, geometry, and proximity metrics to achieve a satisfactory model from contours that define the boundary of regions of interest in the image set. It is also possible to build meshes from the original data by 'detecting' isosurfaces in the data set (i.e., without contour extraction). In this type of approach, the series of original images are piled up to form a volume, and each volume unit is checked for surface intersection [20], [35]. The resulting models obtained from isosurface detection have additional problems than those built using contours. Meshes are too large, details have poor representation, and defining if a particular face of the mesh is 'inside' or 'outside' regarding a particular surface is a difficult task [28]. The reconstruction technique employed in this work falls into the heuristic category, and the metric used for mesh refinement has a topological nature, more robust for computational implementation. The choice of this method was determined by the characteristics of the mesh formed, which is volumetric with comparatively low number of cells, and the aspect of the model makes it adequate for simulation and visualization, as shown in previous works [28], [26].

One novel result on the applicability of the 3D models generated by this methodology is related to the validation of the mesh formation based on the calculation of the volume of the reconstructed parts. An estimation of the error for the reconstruction process supports the use of the methodology in a number of applications in agriculture and elsewhere. To validate volume calculation, two phantom objects were used, for which precise volume measurements were known. One was shaped as a sphere and the other was constructed with a more complex, cube-shaped geometry. By submitting these objects to the three-step procedure the reconstruction error was obtained.

In order to demonstrate the potential of the tools put forward in this work for agricultural applications, measurements of a mango disease, the internal collapse (*Mangifera indica L.*) were computed and analyzed. This disease is characterized by disintegration and de-coloration of the pulp, with loss of its natural consistency. It makes the fruit partially or totally inadequate for consumption. Symptoms are the disintegration of the vascular system in the region of bond between peduncle and endocarp, while the fruit is still in the tree. This causes the seed to be physically and physiologically insulated from tissues that keep them together and gives rise to voids between the regions of the peduncle and endocarp, so that tissues around this empty space start to lose color. The same occurs to the pulp, which also begins to lose color, mainly near the endocarp [8]. These features were not measured with precision before, and it is our expectation that being able to do so will open new frontiers in the study of this problem as well as others in agriculture.

An additional example of applicability of the technique is the volumetric reconstruction of the cashew nut. The goal with the reconstruction of this fruit is to build a geometrical model that will be useful to simulate forces applied during extraction of the almond. In this case the precision of the model is essential for the reliability of the numerical simulation involved.

The next several sections cover each step of the process in turn. It is not our intent to give detailed description of the individual techniques employed, rather to offer an overview of the various techniques employed, and to reflect the work performed in tuning and validating these techniques for the applications presented. This is followed by the method used for validating the volume reconstructed and by the results of the work.

3 2D Imaging

3.1 Magnetic resonance in fruits

An MRI experiment has as result a signal map of the hydrogen (1H) present in the analyzed sample, making it possible to distinguish differences in density and mobility of 1H nuclei. In fruits, these signals essentially come from 1H in free water molecules ($\approx 95\%$). When nuclei, which have magnetic moments, are subjected to an external magnetic field, they align in different energy levels. For 1H, the nuclear spin $\frac{1}{2}$ will have two possible orientations with respect to the external field: parallel or anti-parallel. The difference in energy between these two levels is proportional to the external magnetic field strength. Like other spectroscopic methods, the purpose is to induce transitions between energy levels to obtain a non-equilibrium state. Then, relaxation to equilibrium is observed and recorded. MRI images are obtained by applying radio-frequency pulses at the Larmor frequency of 1H nuclei, adequately combined with magnetic field gradient pulses. Such pulses provide the location of the plane under observation as well as its thickness and its 1H nuclei distribution.

3.2 Data Acquisition

The images used in this work were obtained with the Varian 2 Tesla Magnetic Resonance Imaging System at Embrapa Agriculture Instrumentation, São Carlos (SP), Brazil. Forty-six equally spaced magnetic resonance images of each fruit were collected in the sagittal orientation. MRI images of intact and diseased fruits were acquired using a birdcage radio frequency coil, with a diameter of 14 cm and 30 cm in length, at a proton resonant frequency of 85.5 MHz. Data was acquired using the Spin-Echo Multi Slice pulse sequence, with a 2s repetition time and an 0.015s echo time. Slices were 0.2 cm thick with no gap between slices. Acquisition time for the complete set of 46 tomograms was approximately 12 minutes. Because the signal to noise ratio is high, a single-pass is sufficient for acquiring data. Complex data points were acquired from this system by a workstation, producing a 256x256 pixels image. A 2D Fourier transform converted the original image to a magnetic resonance image. Two examples of MRI images of mangos with corresponding photographs can be seen in figure 1. A dark region means absence of 1H, while the white regions indicate presence of "free" 1H. The several gray shades indicate the regions in which 1H has low mobility. Experiments were carried out on mangos of the variety Tommy Atkins (*Mangifera*

indica, L.). The same process was applied to the validation phantoms (see validation section), and to other fruits.

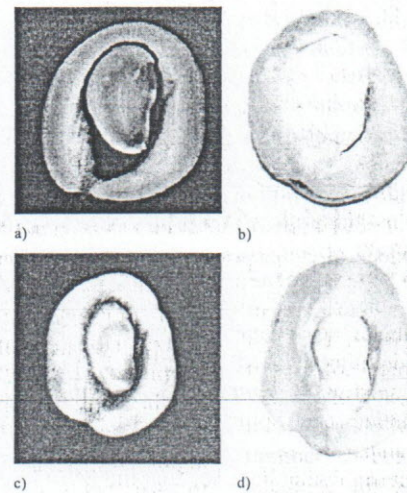


Fig. 1 a) One MRI slice of a mango presenting an internal collapse disease. b) Digital photograph of the mango slice in figure 1a. c) One MRI slice of a healthy mango for comparison. d) Digital photograph of the slice in figure 1c.

4 Image Segmentation

In 3D reconstruction, the boundary curves (contours) of the interest region segmentation need to be detected to be used as inputs for constructing a three-dimensional model. Describing the interior of these areas is also useful.

The segmentation technique employed here is region-based and relies on a homogeneity function to partition the image into regions. The overall idea of this type of segmentation algorithm is to verify, from an initial chosen region (or seed) in the image, if each neighboring pixel to this region should be added to it. The process continues, until there are no more neighboring pixels to be attached to the region. In the case of the images for the mango collapse, seeds for inside and outside regions were chosen individually for core, hole, and pulp.

The algorithm described in [27] employs a similarity function to decide if a neighbor pixel p should be added to a region R . This function associate, to each pair of regions R_{in} and R_{out} , a real value between 0 and 1, where R_{in} and R_{out} are the neighborhoods of p located respectively inside and outside R . If the value of the similarity function is close to 1, then p must be added to R . In this work, the similarity function used was:

$$\Phi(R_{in}, R_{out}) = \frac{1}{\exp\left(\frac{(E(R_{in}) - E(R_{out}))^2}{\sigma^2}\right)} \quad (1)$$

Where E represents the mean of pixel values within each region and σ^2 is the variance of the values in $R_{in} \cup R_{out}$. The algorithm is based on the concept of digital planar surfaces, defined as the union of a set of 8-connected disjoint regions

planar cells [40]. To add a cell (or pixel) p to R , the algorithm employs a set of Morse operators that controls the topology and the boundary curves of R . There is a set of 5 classes of operators named k -handles used to construct the surface by adding one cell ($-1 \leq k \leq 3$). It can be proven that given an object S with Euler characteristic $\chi(S)$ and a k -handle σ then $\chi(S \cup \sigma) = \chi(S) - k$. This property gives control over the topology of the region (and boundary) during construction. With this capability, it is possible, for instance, to control the number of holes in a region. If there is previous knowledge of the expected shape of the region under construction, as in the case of some of the problems studied, the procedure is capable of 'filling out' undesirable holes in the object thus eliminating noise. Other examples of similarity functions and a precise definition of all Morse operators for digital planar surfaces can be found in [27].

An additional advantage of this segmentation algorithm is the fact that, at the same time that it separates regions in the image, it also provides well defined curves representing their contours. Figure 2 illustrates segmentation of the image in figure 1a.



Fig. 2 Contours extracted from image in figure 1a.

Before further processing, the bordering curves generated were simplified by point reduction, to avoid an excessive number of geometric primitives in the final model. The algorithm used takes into account the curvature along the contour [15].

5 3D Reconstruction and Visualization

The reconstruction algorithm employed in this work was based on Delaunay 3D Reconstruction [26]. It begins by generating a 3D Delaunay triangulation [11] from the oriented set of contour points. It then classifies the formed tetrahedrons as internal, external or on the contours, in accordance with their position. Next, reverse tetrahedrons are identified. These are tetrahedrons that have just one edge in each slice, without being contour edges. They appear every time two contours are well positioned geometrically [26], giving an extremely useful heuristic for branching and merging. These reverse tetrahedrons are therefore used to determine which contours should be connected. Then, external tetrahedrons between components are eliminated to disconnect them. The technique also includes procedures to ensure the model is consistent with the original contours and avoid singularities so that they can be used for numerical simulation. Adaptive refinement however would be a useful additional feature [30]. Interactive exploration benefits from the algorithm because the resulting mesh is not as large as those created by other methods. The technique was qualitatively

compared before with traditional isosurface construction approaches [28] and to other Delaunay based reconstruction techniques [40], presenting some advantages. Figure 3 shows the resulting model built for the mango in this study.

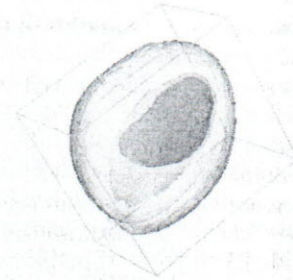


Fig. 3 Model of the three objects of interest in the mango, reconstructed from planar MRI slices.

The basic visualization software used is VTK - The Visualization Toolkit [33] which is an extensible library that implements many visualization methods.

Before proceeding to analyze the results of modeling and visualizing 3D structures in the diseased mango, a validation procedure was carried out using two real life objects, for which the volume could be calculated with high precision. This validation procedure, described in the next section, estimates the reconstruction error.

6 Validation Regarding Volume Calculation

It is important to know how reliable are the models obtained by reconstruction, although this is rarely discussed in the literature. Important issues when judging reliability refer to the aspect of the model and of its individual cells. The most desirable features in a modeling mesh are: absence of singularities, consistency with original object slicing, reduced number of cells and cell aspect ratio. These features are intrinsic of the reconstruction method [26]. An additional piece of information to validate its use for a number of applications is its effectiveness for volume calculation. This would indicate adequacy of the model to define well the region inside the object boundaries. In the case of fruit diseases it would be possible to estimate the portion affected.

A useful method for the purpose of validation employs an object with known geometry and volume, called a 'phantom'. Because the exact internal dimensions of a particular phantom and the value of its volume are known, it can be compared with the volume calculated from a reconstructed version of the same phantom. Due to the large number of approximations used in the reconstruction process, a certain degree of inaccuracy is expected. A measurement of this inaccuracy is the target of the validation procedure.

For the methodology presented here, two phantoms were employed, to account for two different geometrical forms. A cubical phantom (see figure 4) was designed and built using small plates of polymethylmethacrylate. A spherical phantom (a table-tennis ball) was also used. Both phantoms were filled with 1% water solution of Copper Sulphate

(Cu₂SO₄), to lower the relaxation times T1 and T2 below the values for tap water, imaged using the same MRI acquisition method described above, and processed by the same set 3-D reconstruction procedures applied to the mango. The cubic phantom was built with a designed volume of 108.0 cm³, while the actual amount of water solution of copper sulphate it was capable of holding was 107.84 cm³. The sphere had an external diameter of 3.76 cm, with an external volume of 27.83 cm³ and filled volume of 25.95 cm³. Both phantoms were 'sliced' every 0.2cm with no gap between slices (same approach as with the mango). No steps were taken to reduce error during the various phases of the procedure.

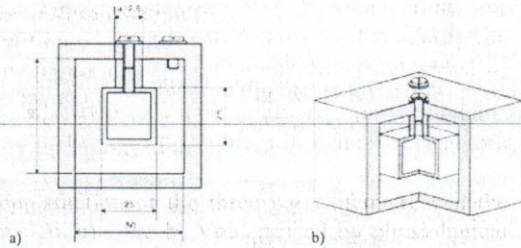


Fig. 4 Phantom, designed and built to validate volume calculation from reconstructed models.

7 Results and Discussion

Applying MRI to investigate the internal quality of fresh fruits is a natural and very important extension of its historical introduction in medicine as an imaging technique for diagnosis [13], [21], [12], [25]. The main advantage of MRI over other investigative approaches is its non-invasive and non-destructive nature. Figure 1a presents a sagittal tomography of a mango with tissue collapse. The core, the void, and the pulp are all visible. Figure 1b presents a digital photograph of the same mango opened with a hacksaw approximately at the same location. Figures 1c and 1d illustrate a healthy mango for comparison. Because there is no tissue collapse in the healthy mango, the dark gray regions around the core (figure 1c) are due to the weak magnetic resonance signal from the low mobility ¹H of the external solid and dry tissues of the core. Due to the nature of the segmentation process used here, that gray region, if segmented, could be interactively included either in the core or in the pulp region, at user's choice. Including it in the core would be the correct choice.

The method employed here for segmentation behaves particularly well when boundaries have uniform intensities over their complete extent. For instance, the separation between hole and pulp to the right of the core in figure 1a is well captured by the method (see figure 2), even where the actual boundary is just slightly visible (that is, dark regions are visually mixed with clear regions). Depending on user needs, either of the attained properties (region or contour) can be used. In this case, we used all the contours generated by the segmentation procedure for every slice, that is, the boundary curves presented in black in figure 2.

From the contours extracted in the whole set of slices, a model was built for the parts of interest in the fruit, which was further explored. One set of models, formed by

processing all frames with three regions of interest (pulp, hole and core), is presented in figure 5, and the triangular mesh of its exterior part is shown in figure 6. This geometric model was used for interaction, analysis and calculation. It is actually composed of tetrahedrons though on the screen only the boundary of the model is displayed. Figure 7 shows a part of the reconstruction of one of the phantoms to illustrate this property. Volume calculations involved summing the volumes of each of its internal tetrahedrons.

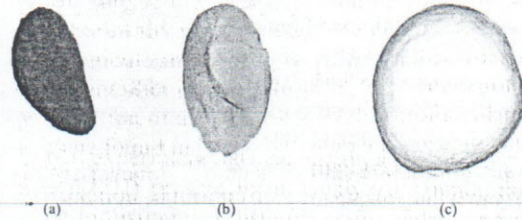


Fig. 5 Reconstruction of the three parts of interest in the diseased mango. a) Core b) Void caused by physiological disturbance. c) Pulp.

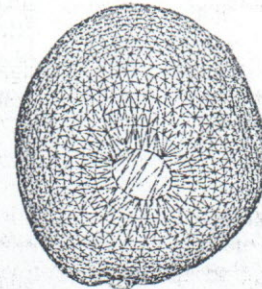


Fig. 6 Mesh for the exterior surface of the mango.

A model was created for each of the phantoms described previously (figure 8b and 8d) using the same scanning parameters as for the mango (see figure 8a and 8c for particular slices). For MRI scanning of the cubic phantom, it was placed at a 45-degree inclination to the equipment axis. The approximations imposed by the reconstruction process have a visual effect in the resulting models, which can be observed in figure 8b. For the cubic phantom, 23 slices were generated, while for the sphere, 19 slices were produced.

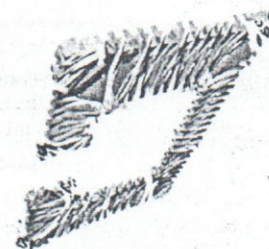


Fig.7 Tetrahedrons in a reconstructed object. A shrinking algorithm was used to split the individual tetrahedrons apart.

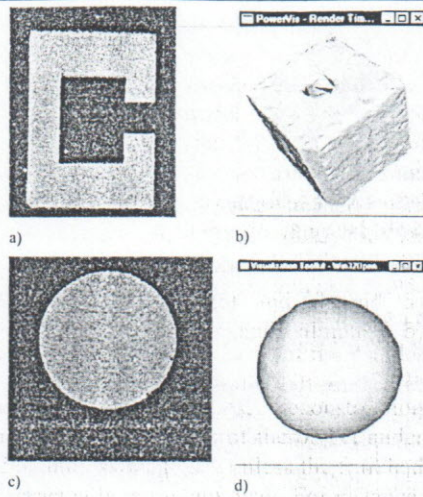


Fig.8 Phantom reconstruction. a) MRI of the cubic phantom. b) reconstructed model for the cubic phantom. c) MRI of the spherical phantom. d) reconstructed model for the spherical phantom.

The volume of the reconstructed spherical phantom was 0.15% higher than the actual sphere and the volume of the cubical phantom was 2.3% higher than the actual volume of the original object (25.988447 cm³ for the sphere and 110.25 cm³ for the cubic object). The number of tetrahedrons is an indication of the size of the mesh and therefore of the time needed to calculate volumetric properties. The number of tetrahedrons generated here (2565 for the sphere, 7636 for the cube, and 11081 for the whole mango) can be handled easily by most computers running the software, and the processing time for volume calculation is not a significant portion of the full process. The void caused by the disease in the studied case was calculated to be 4.04% of the volume of the mango. Because the pulp is 92.47% of the mango, the collapsed part would correspond to 4.37% of the volume of the pulp. The resulting values for the volumes were considered satisfactory, taking into account that errors can occur in many parts of image manipulation, including acquisition (for instance, there is always a slice of the object missing from each end of the image set). Therefore, errors of 0.15 to 2.3% were found for the phantoms. So, if the segmentation process for the application of fruit analysis is acceptable, it is possible to have the same rates of errors in the reconstruction, especially because it was reduced noise in the intermediate steps of reconstruction. If more accuracy is needed, approximation errors could be reduced by a series of extra precautions during processing, such as mesh smoothing, active noise reduction and control of approximation error.

An additional model, for the case of a cashew nut (see figure 9) was also built. The intention with this model is to use its geometric representation to simulate forces on the nut during the extraction of the almond. By studying its behavior under such forces, it may be possible to manufacture a device to improve the unsatisfactory manual extraction process currently used.

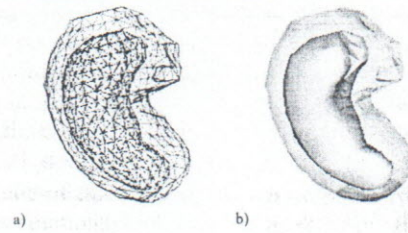


Fig.9 Reconstruction of a cashew nut and almond. a) boundary of meshes of both nut and almond. b) Visualization of the cashew nut.

Besides providing 3D measurements, reconstruction models can also provide internal views of the object under analysis that would be impossible to see unless the fruit had been sliced, diced, or actually cut in any way. For instance, figure-10 shows some manipulation of the model using an interactive technique implemented in the system. A 'cursor' is used to mark a path on the fruit surfaces, starting with the external object. When the path is closed, the surface enclosed by it can be 'cut', and the cut can be treated as a separate object (figures 10a to 10d). This object can be manipulated separately, or even deleted from the scene. With this 'opening', the user can actually walk through the mango and explore its structures internally. The process can be repeated for internal objects. Figure 10e illustrates the view of the core through cuts in both the external object and the hole. This technology allows nonphysical operations and insights that would be impossible in the real world, such as 'seeing a hole in 3D', or even 'cutting a hole' to see the core. This flexibility could be useful for a number of known or novel applications.

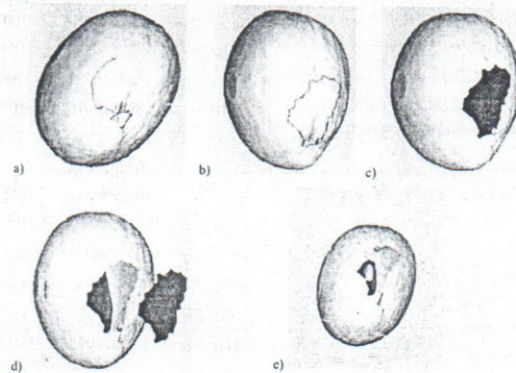


Fig.10 Various levels of interaction with the mango models.

8 Conclusions

The methodology developed in this work represents an innovative contribution where the reliability of 3D model construction is important. First, because it covers the whole process from acquisition to model manipulation, offering detailed instruction for potential users. Second, because it validates the model created against volume calculation, a quality missing in other reconstruction efforts which has restricted their use.

The qualities inherent of the segmentation and reconstruction methods were favorable here. In the segmentation algorithm, the topological control over the surface construction speeds up the reconstruction process. By having an idea of the shape of the objects undergoing reconstruction it was possible to eliminate noisy regions in the data while maintaining the actual 'holes' that were part of the structure under analysis. In the volume reconstruction step, the topological tests and the quality of the mesh formed gave robustness and good definition of the object formed.

Many areas in agriculture can benefit from the use of the developed methodology. Examples include study of diseases in fruits, analysis of structure of fruit elements (as in the cashew nut case), study of soil behavior and analysis of factors that influence fat and water content in meat, to mention a few. For instance, the accuracy of the 3D mesh is necessary to allow a reliable simulation of the forces applied on the cashew nut during extraction of the almond. This work has just started with the reconstruction of cashew models. In the case of soil, a study is being planned for development of a metric of porosity through the calculation of volume of capillaries reconstructed from soil samples. As for the mango, the measurement of volume of tissue collapse serves as starting point for the development of a biophysical model that describes the phenomenon. This model, together with additional data on mango plantations could support the description of the evolution of the disturbance and guide the manipulation of the problem therein.

Being the only methodology for 3D reconstruction currently that had the volume calculation validated, it is expected that the contribution presented here will have application in many other fields of science. This aspect, added to the intrinsic qualities of the volumetric model generated by the reconstruction method, allows for expansion of its use for other applications, such as medical.

It must be noticed that the methodology requires good quality images for its accuracy, reason why the use of MRI is important as the acquisition method. Low quality images that produced noise on the boundary of the regions of interest would generate imprecise contour definition, impairing the creation of reliable models.

Besides providing a full methodology for data manipulation from image to interaction, this work gives a contribution for the discussion of validation of reconstruction methods, particularly in the case where volume calculation is of concern.

References

1. Beutel, J., Kundel, H., Van Metter, R. L. (Eds.), 2000, Handbook of Medical Imaging, 1, Physics and Psychophysics, SPIE Press.
2. Baraldi A., Parmiggiani F., 1996. Single linkage region growing algorithms based on the vector degree of match. IEEE Trans. on Geoscience and Remote Sensing, 34(1), 137-148.
3. Boissonnat, J-D., 1988. Shape reconstruction from planar cross sections, Computer Vision, Graphics and Image Processing, 44, 1-29.
4. Bouman, C., 1995. Markov Random Fields and Stochastic Image Models. Tutorial presented at IEEE Inter. Conf. on Image Processing, Washington, 23-25.
5. Canny, J., 1986. A computational approach to edge detection. IEEE Trans. Pattern Anal. Machine Intell., 8, 679-698.
6. Clark, C.J., Burmeister, D.M., 1999. Magnetic resonance imaging of browning development in 'Braeburn' apple during controlled-atmosphere storage under high CO₂. Hortscience, 34(5), 915-919.
7. Clark, C.J., Hockings, P.D., Joyce, D.C., Mazucco, R.A., 1997. Application of magnetic resonance imaging to pre and post-harvest studies of fruits and vegetables. Post-harvest Biol and Technol, 11, 1-21.
8. Cunha, M.M., Santos-Filho, H.P., Nascimento, S.A. (Org.), 2000. Manga: Fitossanidade. Brasília, DF: Embrapa Comunicação para Transferência de Tecnologia.. Chapt 5, 71-73.
9. Ekoule, A. B., Peyrin, F. C., Odet, C. L., 1991. A Triangulation Algorithm from Arbitrary Shaped Multiple Planar Contours, ACM Trans. on Graph., 10(2), 182-199.
10. Fitzpatrick, J. M., Sonka, M. (Eds.), 2000. Handbook of Medical Imaging, Volume 2, Medical Image Processing and Analysis, SPIE Press, Washington DC, USA.
11. Fortune, S., 1994. Voronoi Diagrams and Delaunay Triangulation. Computing in Euclidean Geometry. Du, D-Z., Hwang, F.K. (Eds.), World Scientific Pub. Co., 193-233.
12. Foster, M.A., 1984. Magnetic resonance in medicine and biology. Pergamon, Oxford, U.K.
13. Gadian, D.G., 1982. Nuclear magnetic resonance and its applications to living systems. Oxford Univ. Press, Oxford, U.K.
14. Gonzalez, J.J., Valle, R.C., Bobroff, S., Biasi, W.V., Mitcham, E.J., McCarthy, M.J., 2001. Detection and monitoring of internal browning development in "Fuji" apples using MRI. Post-harvest Biol. and Technol., 22, 179-188.
15. Hamann B., Chen J-L., 1994. Data point selection for piebewise linear curve approximation. Computer Aided Geometric Design, 11, 289-301.
16. Haris K., Efstratiadis S., 1998. Hybrid Image Segmentation Using watersheds and Fast Region
17. Merging. IEEE. Trans. on Image Processing, 7(12), 1684-1699.
18. Kato Z., 1994. Multi-scale Markovian Modelisation in Computer Vision with Application to SPOT Image Segmentation, PhD Thesis, Universtity of Nice.
19. Kim, Y., Horii, S. C. (Eds.), 2000. Handbook of Medical Imaging, Volume 3, Display and PACS, SPIE Press, Washington DC, USA.
20. Lorensen, W. E., Cline, H. E., 1987. Marching Cubes: A high-resolution 3D surface construction algorithm. ACM SIGGRAPH Computer Graphics 21(4), 163-168.
21. Mansfield, P., Morris, P.G., 1982. NMR imaging in biomedicine. Academic Press, New York.
22. Van Metter, R. L., Beutel, J., Kundel, H. L. (Eds.), 2000. Handbook of Medical Imaging, Volume 1.

- Physics and Psychophysics, SPIE Press, Washington DC, USA.
23. Meyers D., Skinner, S., Sloan, K., 1992. Surface from Contours, ACM Trans. on Graphics, 11(3), 228-258.
 24. Monga, O., Deriche, R., Malandain, G., Cocquerez, J.P., 1991. Recursive filtering and edge tracking: Two primary tools for 3D edge detection. Image Vis. Comput., 9(4), 203-214.
 25. Morris, P.G., 1986. Nuclear magnetic resonance in medicine and biology. Oxford Univ. Press, Oxford, U.K.
 26. Nonato, L.G., Minghim, R., Oliveira, M. C. F., Tavares, G., 2001a. A Novel Approach for Delaunay 3D Reconstruction with a comparative analysis in the Light of Applications. Computer Graphics Forum., 20(2), 161-174.
 27. Nonato, L.G., Castelo, A., Minghim, R., Batista, J.E.S., 2001b. Morse operators for digital planar surfaces and their application to image segmentation. IEEE Transactions on Image Processing, 13(2):216-227, 2004.
 28. Nonato, L.G., Minghim, R., Shimabukuro, M.H., 2000. Qualitative Analysis of two Reconstruction Techniques and their application in Dentistry. Journal of Electronic Imaging, 9(4), 385-393.
 29. Pal, N., Pal, S., 1993. A review on image segmentation techniques. Pattern Recognition, 26, 1277-1294.
 30. Shewchuk, J. R., 1998. Tetrahedral Mesh Generation by Delaunay Refinement. Proceeding of 14th. Annual Symposium on Computational Geometry, ACM Press, 86-96.
 31. Shimabukuro, M. H., Minghim, R., Licciardi, P.R.D.B., 1998. Implementing Visualization Procedures in Dental Applications, Proceedings of Information Visualization '98, London, UK, IEEE CS Press, pp.25-31.
 32. Shinagawa, Y., Kunii, T. L., 1991. The homotopy model: a generalized model for smooth surface generation from cross sectional data, The Visual Computer, 7, 72-86, 1991.
 33. Schröder, W.J., Martin, K., Lorensen, W., 1998. The Visualization Toolkit, An Object-Oriented Approach to 3D Graphics. 2nd ed. Prentice-Hall, Englewood Cliffs, NJ.
 34. Singh, A. Goldgof, E., Terzopoulos, E. (Eds.), 1998. Deformable Models in Medical Image Analysis, IEEE CS Press.
 35. Treece, G. M., Prager, R. W., Gee, A. H., 1998. Regularised Marching Tetrahedra: Improved Esosurface Extraction, CUED/F-INFENG Technical Report 333, Cambridge University Engineering Department.
 36. Thomas, P., Kannan, A., Dgwekar, V.H., Ramamurthy, M.S., 1995. Non-destructive detection of seed weevil-infested mango fruits by X-ray imaging. Post-harvest Biol and Technol, 5, 161-165.
 37. Wang, C.Y., Wang, P.C., 1989. Nondestructive detection of core breakdown in "Bartlett" pears with nuclear magnetic resonance imaging. Hortscience, 24(1), 106-109.
 38. Wang, C.Y., Wang, P.C., Faust, M., 1988. Non-destructive detection of watercore in apple with nuclear magnetic resonance imaging. Scientia Horticulturac, 35, 227-234.
 39. Xu, C., Pham, D.L. and Prince, J.L., 2000. Image Segmentation using Deformable Models. in Fitzpatrick, J. M., Sonka, M. (Eds.), Handbook of Medical Imaging, 2, chapt. 3. SPIE Press.
 40. Nonato, L.G., Castelo, A., Campos, J.E.P.P., Biscaro, H.H., Minghim, R. Topological Tetrahedron Characterization with Application in Volume Reconstruction. International journal of shape modeling, 11(2):189-216, 2005.

L.A.C. Jorge, C.I. Biscegli

Embrapa Instrumentação Agropecuária, Rua 15 de Novembro, 1452, C.P. 741, 13560-970, São Carlos, SP - Brazil

Tel.: +55-16-33742477

Fax: +55-16-33725958

E-mail: lucio@cnpdia.embrapa.br; clovio@cnpdia.embrapa.br

R. Minghim, L.G. Nonato

Departamento de Ciências de Computação e Estatística, ICMC-USP, Avenida Trabalhador São-carlense, 400 - C. P. 668, 13560-970, São Carlos, SP, Brazil

E-mail: rminghim@icmc.usp.br; gnonato@icmc.usp.br

V.O. Roda, E.C. Pedrino, M.S.V. Paiva

Departamento de Engenharia Elétrica, EESC-USP

Avenida Trabalhador São-carlense, 400 - 13566-590 - São Carlos, SP, Brazil

Tel.: +55-16-33739371

FAX: +55-16-3373 9372

E-mail: valentin@sel.eesc.usp.br; ecpedrino@terra.com.br;

mstela@sel.eesc.usp.br